JAAS

Parametric Optimization and Spectral Line Selection for Liquid Sampling – Atmospheric Pressure Glow Discharge – Optical Emission Spectroscopy

Journal:	*Journal of Analytical Atomic Spectrometry*
Manuscript ID	JA-ART-09-2019-000325.R1
Article Type:	Paper
Date Submitted by the Author:	22-Oct-2019
Complete List of Authors:	Hall, Katja; Clemson University, Chemistry; Clemson University Marcus, R.; Clemson University, Chemistry

Parametric Optimization and Spectral Line Selection for Liquid Sampling – Atmospheric Pressure Glow Discharge – Optical Emission Spectroscopy

Katja A. Hall and R. Kenneth Marcus*

Submitted for publication in the

Journal of Analytical Atomic Spectrometry

Department of Chemistry
Biosystems Research Complex
Clemson University
Clemson, SC 29634

* Author to whom correspondence should be addressed

Abstract

A design-of-experiment (DOE) parameterization was performed with the liquid sampling – atmospheric pressure glow discharge (LS-APGD) optical emission spectrometry (OES) system to establish the optimal powering mode and operating conditions that allow for maximum signal intensity, signal-to-background (S/B) ratio, and signal-to-noise (S/N) ratio. Different from other APGD sources, the operation principles of the LS-APGD provides alternative means of applying the discharge potential. As a result of this parameterization, the sensitivity of the LS-APGD was dramatically improved, as noted by the ~30x improvement in limit of detection (LOD), now 0.8 μg mL^{-1}) for 20 μL injections, versus earlier reports, with the solution-grounded cathode (SGC) found to be the preferred powering mode. Using the parameters from the DOE analysis, a line selection evaluation was performed for Ag, Ca, Cr, Cu, K, Mg, Na, and Zn as test elements. The best emission lines for analytical performance determination and future works were determined by measuring the stability and signal intensity for all observed lines. The chosen lines were probed for sensitivity by acquiring calibration curves for each of the analytes' transitions. When single-element solutions were used, the LODs acquired for many of the analytes were superior to previously reported LS-APGD results. While the sensitivity of the LS-APGD-OES is lower than that of an ICP-OES, the LODs for the LS-APGD are likely acceptable for those applications where portability and low-cost instrumentation are desired.

Introduction

Inductively coupled plasma optical emission spectroscopy (ICP-OES) has been the benchmark technique for multi-element optical emission analysis for decades.[1] It is widely used across various scientific disciplines due to its advantageous features, including wide linear dynamic range, relatively-low detection limits, and simultaneous multi-element capabilities.[2] ICP-OES is however, limited in many ways, such as the high power requirements (1-2 kW), high support gas flow requirements (>15 L min^{-1} Ar), and large sample volumes (~ 5 mL), of which most goes to waste.[2, 3] These operating requirements as well as the large initial cost of the instrument and high maintenance/operation costs drive continuous evaluation into alternative sources.

To address the operational overhead and high costs associated with ICP techniques, recent research in the field of atomic spectroscopy has focused on the miniaturization of excitation/ionization sources.[4] Potential benefits could be the use of less sample, less waste production, more efficient operation, and portability. The ideal products of this research would be instruments capable of performing at or near the level of ICP-OES. Towards this end, a promising area of research lies in the development of atmospheric pressure glow discharge (APGD) sources. The initial demonstration of these APGD sources was the electrolyte cathode atmospheric glow discharge (ELCAD) developed by Cserfalvi *et al.*[5] The ELCAD, and excitation sources based off its design, is a promising alternative to the ICP due to its low power requirements, low-cost, and ability to operate under ambient conditions.[6-10] Several APGD sources based on the ELCAD exist, and the various approaches to generating these sources have been well reviewed.[6, 11, 12] A notable improvement on the original

ELCAD design is the solution cathode glow discharge (SCGD) demonstrated by Hieftje and collaborators.[13, 14] In particular, aspects of using 10s of microliter volume sample injections into the bulk flow and the use of spatially-segregated optical sampling were demonstrated.

The liquid sampling – atmospheric pressure glow discharge (LS-APGD) was developed by Marcus and Davis as an alternative to the ELCAD design and offers several advantages over both the ICP and other APGD sources.[15] The LS-APGD has lower capital costs and operational requirements, using less power (<100 W) and support gas (<1 L min^{-1}) than the ICP. In comparison to ELCAD-type devices, far less sample is used (<0.1 mL), and no liquid waste is produced by virtue of low solution flow rates (<100 μL min^{-1}) and high power densities (>10 W mm^{-3}).[15, 16] The LS-APGD also has wide-ranging utility, as it can pair with OES, atomic mass spectrometry (MS), and molecular MS.[17-23] Solids can be sampled *via* ambient desorption (AD) and laser ablation (LA) for OES/MS analysis.[21, 22, 24, 25] The lack of liquid waste generation and versatility of detection modes is a distinct advantage of the LS-APGD over other APGD sources which operate at much higher liquid flow rates and are typically paired solely with direct liquid sampling and OES detection,[13, 14, 26-29] though the SCGD has also been applied for atomic MS.[30]

While the utility of the LS-APGD has been demonstrated and its potential advantages relative to other sources are defined, the LS-APGD still struggles with limited concentration-based sensitivity when used for OES measurements.[31] Previously reported limits of detection (LOD) have been suitable for trace metal analysis but ill-suited for ultra-trace metal analysis.[32] For those applications requiring high sensitivity,

in-line sample preconcentration has been performed to improve measurement sensitivity.[31] However, more progress is necessary if the LS-APGD-OES system is to be reasonably offered as an alternative for ICP-OES. In reality, for cases of reduced-format analytical instrumentation, ICP-OES-level sensitivity may be worth sacrificing for a cost-effective instrument with fewer operational requirements and the potential to perform at-sample (transportable) analysis.

Described in this work is a comprehensive parameterization of the LS-APGD operation conditions followed by a line selection and analytical characterization, with the goal of improving the analytical performance of the LS-APGD-OES system. A reduced-format monochromator and PMT were used for this work due to the sensitivity, moderate resolution, wide wavelength range, and low cost. The parameterization was performed with a solution of 500 μg mL^{-1} Ag to remain consistent with previous LS-APGD literature.[31] The parameterization was performed using the four possible LS-APGD powering modes in order to determine which provides optimal response. The test elements for the line selection and analytical characterization were Ag, Ca, Cr, Cu, K, Mg, Na, and Zn. These elements were chosen based on their appearance in the literature for previous characterization of the LS-APGD, their use for the development of other APGD sources, and their diversity of spectrochemical characteristics.[12, 17, 33]

Experimental

Liquid Sampling – Atmospheric Pressure Glow Discharge Source - The LS-APGD-OES apparatus, depicted in Fig. 1, remains essentially unchanged from recent iterations.[31, 34] A Chemyx Fusion 100 syringe pump (Stafford, TX) was used to transport an electrolytic solution (5% HNO_3) through a fused silica capillary (i.d. – 280 μm, o.d. – 580 μm,

Restek (Bellefonte, PA)) to sustain the plasma. This capillary was mounted inside of a stainless-steel outer electrode, with a He sheath gas flowing through it. Sheath gas was delivered using a mass flow controller (Alicat Scientific MC Series (Tucson, AZ)). Mounted opposite to this electrode (the solution electrode) was a second, identical electrode (the counter electrode). This electrode is hollow to facilitate the introduction of a He counter gas flow, controlled with an identical mass flow controller.[31, 34, 35] The plasma was powered by a direct current power supply (Spellman Model SL 150, Hauppage, NY) with a 10 kΩ ballast resistor placed between the power supply and the counter electrode.

LS-APGD Powering Modes - A glow discharge is formed based on the potential difference applied between two electrodes. The power supply used to sustain the LS-APGD can operate in either a positive or negative output mode, and the solution electrode can be either powered or grounded, meaning the LS-APGD can be powered in four different ways,[36] a unique feature versus other APGD types. Diagrammatic representations of each of these powering modes is shown in Fig. 2.

Solution Preparation – Concentrated, trace metal grade, nitric acid (Sigma-Aldrich (St. Louis, MO)) was diluted to 5% v/v using DI-H_2O (Purelab Flex, ELGA Waterlab, High Wycombe, UK). The 5% HNO_3 solution was used to prepare each of the analytes from their corresponding salts. All salts were obtained commercially from the following sources: $AgNO_3$ (Fischer Scientific; Fair Lawn, NJ), $Ca(NO_3)_2$*$4H_2O$ (Sigma-Aldrich; St. Louis, MO), $Cu(NO_3)_2$*3 H_2O (Carolina Biological Supply Company; Burlington, NC), $Cr(NO_3)_3$*9 H_2O (Sigma-Aldrich; St. Louis, MO), KCl (Fischer Scientific; Fair Lawn, NJ), NaCl (Alfa Aesar; Ward Hill, MA), $Mg(NO_3)$*6 H_2O (Sigma-Aldrich; St. Louis, MO),

$Zn(CH_3COO)_2$*2 H_2O (J.T. Baker Chemical Co.; Phillipsburg, NJ). Each analyte stock solution was prepared at 500 μg mL^{-1}. The multi-element solution was prepared with the same concentrations of each salt used in the single-element solutions, save for K and Na which were diluted to 100 μg mL^{-1} due to their intense responses, and diluted with 5% HNO_3.

Optical Emission Detection - Light emission from the plasma was focused onto the entrance slit of a CVI Laser Digikrom 240 0.24 m focal length monochromator (Albuquerque, NM) using a tube lens containing two CaF_2 plano-convex lenses (Thorlabs, Newton, NJ). (Note that this a small format spectrometer in comparison to ICP-OES instruments, commensurate with a reduced-format laboratory instrument. Other modalities may be more appropriate for transportable instruments.) While a monochromator is not the ideal choice for a line selection study due to the inability to monitor multiple wavelengths simultaneously, the good resolution across a large wavelength range and low cost warrant its use in this investigation. The focal length of the lens mounted adjacent to the plasma was 150.0 mm and the focal length of the lens on the opposite side of the tube was 40.0 mm. The monochromator employed for this work had 1200 grooves mm^{-1} grating, blazed at 250 nm, and 0.2 nm resolution, with a spectral working range of 200 – 1500 nm. The entrance and exit slits for all experiments were set at 50 μm. All spectral scans acquired in this work were taken at a rate of 100 nm min^{-1} at steps of 0.01 nm. The signal integration time was set to 6 ms per step. A photomultiplier tube (Hamamatsu R955; Bridgewater, NJ) was used as the photon detector and transducer.

Design of Experiment (DOE) Approach for Optimization of Operating Conditions - To optimize the operating conditions of the LS-APGD-OES system, a design of experiment (DOE) study was undertaken to assess the influence of the following parameters: discharge current, inter-electrode gap, sheath gas flow rate, counter gas flow rate, and solution flow rate. While previous parameterizations have been conducted, they have either not included all the listed parameters, studied them in isolation, or have studied these parameters across a limited range. The ranges of conditions used in this DOE study were as follows: discharge current (30 – 70 mA), inter-electrode gap (0.5 – 4.0 mm), sheath gas flow rate (0.5 – 0.9 L min^{-1}), counter gas flow rate (0.1 – 0.5 L min^{-1}), and solution flow rate (25 – 125 μL min^{-1}). While the LS-APGD can operate past the minimum and maximum of these ranges, concessions were made to bring down the computational cost of the DOE as well as reduce the total number of experiments performed. The chosen ranges of parameters do encompass all previously established optimal parameters for the setup, so comparisons can be made between this work and previously-reported data.

Typically, full factorial designs are used in such evaluations, but it is more computationally expensive and requires more combinations of operating conditions.[37, 38] As such, a definitive screening design (DSD) was used. While DSD does not consider as many combinations of parameters as other models, its ability to detect and predict the causes of any nonlinearity justifies its use in this work.[39, 40] A DSD experimental plan was generated using JMP Pro software (Cary, NY). The experimental plan consisted of 22 unique sets of operating parameters, shown in Table 1. Triplicate 20 μL injections of the 500 μg mL^{-1} Ag test solution were performed at each set of operating parameters

listed in Table 1. Ag was chosen as the test element due to its use in previous characterizations of the LS-APGD.[31, 34, 35, 41] While a single element approach represents very much a middle ground, Ag is neither the most or least sensitive of elements by the method, and serves as a suitable test element. (In no case was evidence of self-absorption or PMT saturation seen.) Signals were collected across the injection transients at Ag (I) 328.1 nm, at a rate of 10 per second. The average (integrated) signal intensity across the injection, signal-to-background (S/B), and signal-to-noise (S/N) were calculated from the transients of each injection and input into the JMP Pro software. The S/B was calculated as the maximum intensity divided by the average intensity for one minute before and one minute after the injection. The S/N was calculated as the maximum intensity divided by the standard deviation of the intensity in the same regions before and after the injection. JMP Pro performed statistical calculations to determine the significance of each parameter on the generated model of analyte responses. These significance values are reported in LogWorth ($-\log_{10}$(p-value)), with a value of 1.5 indicating significance at the 95% confidence interval.

To choose the optimal powering mode for the LS-APGD, the DOE outlined in Table 1 was performed for each. The optimal parameters were extracted for each powering mode and triplicate injections of the test solution were performed at those conditions. To determine which powering mode offered the best analytical performance, the signal intensity, S/B, and S/N for these conditions were compared.

Line Selection - The line selection was performed using the optimal operating conditions obtained from the DOE method. Eight analytes (Ag, Ca, Cu, Cr, K, Na, Mg, Zn) were chosen for evaluation based on their use in previous characterizations of the LS-APGD

and other APGD sources, as well as diversity in terms of both wavelengths and the identity of the emitting species (i.e., atomic *vs* ionic). To evaluate the transitions from each analyte, full spectra (200 – 800 nm) were acquired using constant flow solutions while introducing 500 μg mL^{-1} of each element, individually. Corresponding background spectra were acquired across the same spectral region using a constant flow of the 5% HNO_3 blank solution. Background corrections were performed by subtracting the full background spectrum from the analyte spectrum on a point-by-point basis. This process was performed in triplicate with three unique analyte and background scans. Any remaining transitions that had been previously attributed to that analyte were identified as potential analytical transitions. The temporal stability and precision for each transition was determined by performing triplicate injections of analyte at each identified line and calculating the %RSD of the integrated peak area, peak height, S/B, and S/N. In this case, the S/B was calculated using the maximum intensity of the analyte peak divided by the average intensity of the background region 0.5 nm below and above the analyte line. The S/N was calculated using the maximum intensity of the analyte peak divided by the standard deviation of the intensity in the same regions. The ultimate analytical line for each analyte was chosen based on these criteria.

Analytical Performance - Calibration curves for each analyte were obtained at the chosen analytical line using the average transient peak height of three, 20 μL injections of each solution. The peak height from each injection was determined by finding the maximum intensity from the transient signal of each injection. These calibration curves were then used to calculate the LOD for each analyte ($3\sigma_b/m$; where σ_b is the standard deviation of triplicate blank measurements and m is the slope of the calibration curve).

This analysis was performed using single-element solutions of each analyte individually as well as the multi-element solution described previously. The multi-element solution was used to determine how the plasma operates with high concentration solutions and to identify potential matrix effects.

Results/Discussion

Design of Experiment Evaluation of Powering Modes –

The DOE outlined in Table 1 was performed in each of the powering modes to determine the optimal conditions for LS-APGD-OES analysis. Each powering mode was evaluated under the same DOE experimental plan. Each parameter was identified as having either a positive, neutral, or negative impact on the responses. Previous works have discussed the significance of each parameter towards the microplasma operation,[17] so this work focuses solely on identifying the effect each parameter has on analytical responses for each powering mode. In those cases where changing a parameter had a positive effect on signal intensity but a negative effect on S/B or S/N, parameters were chosen to obtain the most desirable compromise between the three monitored responses. These situations will be discussed on a per scenario basis as they appear in this work.

Solution Grounded Cathode (SGC) - The SGC powering mode is the powering orientation typically used for ELCAD and SCGD operation.[11, 13] The operating parameters with positive correlations to analyte response in the SGC powering mode were discharge current and counter gas flow rate. Negatively correlating parameters were electrode gap, sheath gas flow rate, and solution flow rate. As shown in the Pareto plot in the Electronic Supplementary Information Fig. 1 (ESI-F1), the

parameters/combination of parameters found to significantly affect analyte response were discharge current * sheath gas flow rate, discharge current, and solution flow rate * sheath gas flow rate. The optimal operating conditions of the LS-APGD based on the above metrics in this powering mode were determined to be: discharge current = 60 mA, electrode gap = 2 mm, sheath gas flow rate = 0.6 L min^{-1}, counter gas flow rate = 0.3 L min^{-1}, and solution flow rate = 25 μL min^{-1}.

Solution Powered Cathode (SPC) - The parameters with a positive correlation to emission intensity, S/B, and S/N were discharge current and counter gas flow rate while negative correlations arose from electrode gap, sheath gas flow rate, and solution flow rate. Counter gas flow rate was found to have a neutral impact on all monitored responses. As depicted in ESI-F2, it was found that no single parameter nor a combination of parameters significantly affected analyte response. The optimized operating conditions of the LS-APGD in this powering mode were found to be: discharge current = 70 mA, electrode gap = 0.5 mm, sheath gas flow rate = 0.6 L min^{-1}, counter gas flow rate = 0.3 L min^{-1}, and solution flow rate = 25 μL min^{-1}.

There has been one previous parameterization of the LS-APGD in the SPC powering mode.[17] The results of that work align closely with the data presented here, except for sheath gas flow rate. In that work, sheath gas flow rate was found to have a positive effect on analyte emission across the same range. In this study however, no correlation to analyte response was found. The previous parameterization found that the effect of sheath gas flow rate on emission intensity was analyte dependent. Additionally, the previous work utilized a substantially higher solution flow rate (150 μL min^{-1}) as it was tailored toward the use of the LS-APGD as a secondary excitation source for

particle analysis.[17] This could influence the outcome of the experiments performed, particularly considering high solution flow rates were found here to have a negative correlation with analyte response.

Solution Grounded Anode (SGA) - The discharge current was found to have a positive correlation to analyte emission intensity, but this is only true up to 40 mA, beyond which increases in current negatively affected emission intensity. S/N and S/B were not affected by discharge current. Every other parameter was found to have a negative impact on all three responses across the entire studied range. The only condition found to have a significant (albeit negative) effect on analyte response was the sheath gas flow rate, as shown in ESI-F3. The optimized operating conditions of the LS-APGD in this powering mode were found to be: discharge current = 40 mA, electrode gap = 0.5 mm, sheath gas flow rate = 0.5 L min^{-1}, counter gas flow rate = 0.1 L min^{-1}, and solution flow rate = 25 μL min^{-1}.

There has been a previous parameterization of the LS-APGD-OES in the SGA powering mode.[41] The results from that work are consistent with this work, with some important distinctions. First, the current was found to have a positive correlation to signal intensity from 25 – 35 mA, but a negative correlation beyond that point. Second, no counter gas was included in the previous work and electrode gap and sheath gas flow rate were held constant. Finally, the previous work used the one-variable-at-a-time (OVAT) method to find the optimal discharge current and solution flow rate. The OVAT method is commonly used, but does not consider inter-parametric effects, which play an important role in plasma operation. Due to this difference and the number of operating parameters studied in the previous work, it is not surprising that the results differ.

Solution Powered Anode (SPA) - When powered under the SPA conditions, the LS-APGD was unstable at every parameter combination generated by the JMP Pro software. Injections were attempted at every condition, but the tip of the solution electrode melted, or the plasma became too unstable for reliable intensity measurements. As such the DOE protocol could not be completed and SPA was deemed unusable. While the plasma is sustainable in SPA mode, the low sensitivity compared to other powering modes aligns with previous results of LS-APGD powering mode studies.[36]

Selection of Powering Mode -

Triplicate 20 µL injections of the 500 µg mL^{-1} Ag test solution were performed using the optimized conditions for each powering mode. The average peak height, S/B, and S/N were calculated for these conditions. Figures 3a-c show the average (integrated) signal intensity, S/B, and S/N for each powering mode, respectively. The error bars on the graphs are the standard deviation (1σ) of the metrics across the triplicate injections. The maximum signal intensity and S/B as well as the lowest dispersion for both were achieved using the SGC powering mode, while the highest S/N was achieved with the SGA powering mode. That said, the variability of the S/N is far greater for the SGA powering mode than that acquired with the SGC powering mode. The responses monitored here were found to be degraded when the plasma was operated in the SPC powering mode due to the comparatively low magnitude and the high deviation of all monitored responses. Based on these data, the plasma was run in the SGC powering mode for the remainder of these studies under the optimal conditions extracted from the DOE study.

To compare the analytical performance of the LS-APGD using the parameters extracted in this study to previous iterations, response curves for Ag (I) 328.1 nm were produced under the microplasma conditions derived here and which had been employed in those works. The resulting response curve is shown in Fig. 4, along with a curve generated using the initial operating conditions of the source[15, 36] and using the conditions from the most recent published calibration effort.[31] The response curves were generated over the same concentration range (10 – 500 μg mL^{-1}) and each calibration curve contains five points. The concentrations used to generate the responses were determined using the random number generator function in Microsoft Excel. While each calibration curve used different concentrations of solution, they are all representative of LS-APGD response over the same concentration range at the specified conditions.

The response curve acquired using the optimized plasma conditions from this work begins to deviate from linearity between 250 and 500 μg mL^{-1}. For this reason, the line of best fit is represented by a second order polynomial function. (Suppression at high analyte loadings is addressed in subsequent sections of this report.) A 14x improvement in slope is observed in the linear response region (<250 μg mL^{-1}) for the conditions found in this study when compared to the initial plasma operation conditions.[15, 36] A 3x improvement in slope was also achieved in the calibration curve at the current conditions *versus* the calibration curve acquired in the most recent publication.[31] When LODs were calculated using these calibration curves, the lowest LOD (0.8 μg mL^{-1}, 16 ng) was acquired using the conditions found here. The LODs using the conditions from Hall *et al*.[31] and Marcus *et al*.[15, 36] were 1.0 and 25.3 μg mL^{-1}, respectively. Using the DOE approach to establish the most suitable operating

parameters for the LS-APGD, based on these response curves, was successful. Further experiments were performed to determine if the parameterization had the effect of improving analytical performance for other analytes.

Analytical Line Selection - The sequential nature of the present monochromator system is non-ideal in terms of multi-line measurements. To ensure greater temporal stability across the time scales required for multiple broad spectral scans, the solution flow rate was increased to 50 μL min^{-1}. This assisted in cooling the solution electrode and inner capillary, allowing for continuous use of the plasma for more than 8 hours with no degradation in performance. The solution flow rate was adjusted instead of the sheath or counter gas flows because, while none of the parameters were found to significantly affect plasma operation, the solution flow rate had the smallest effect on signal intensity and plasma stability when modified. While increasing the solution flow rate did have a slight negative effect on the signal intensity (~10%), S/B and S/N were unaffected, as was the %RSD of all three responses. No other parameters were changed.

The fundamental characteristics of the excitation source used for OES experiments plays a large role in the states that are populated and thus the transitions that are observed in emission spectra.[42, 43] The spectroscopic background (typically water- and atmosphere-related species) also plays a role in the visible region of the spectrum. As such, analytical lines need to be chosen based not only on emission intensity, but also on S/B, S/N, and the reproducibility of these responses. Therefore, the line selection study was performed with two basic experiments. The first was identifying analyte emission lines using constant flow solutions of single- and multi-element solutions. The second was studying the stability of analyte emission lines by

performing multiple injections at each line identified for each analyte and calculating the %RSDs for injection peak area, peak height, S/B, and S/N. The emission lines for use in the analytical characterization of the source were chosen based on these factors.

Previous works characterizing the emission spectra of the LS-APGD have established that the spectra are comparable to those of combustion flames operated at atmospheric pressure.[15, 36] The LS-APGD blank spectra (5% HNO_3, pH = 1) are dominated by molecular band emission from $OH^{\bullet}$, N_2, N_2^+, and NH, which is typical of atmospheric pressure flame sources as well.[43] Additionally, when the rotational temperatures from the $OH^{\bullet}$ Q1 brand were calculated, values of 2300 – 2800 K were acquired, closely following those measured in atmospheric pressure flames.[15] Determinations of excitation temperatures have yielded temperatures of 2700 – 3600 K.[36] Since the rotational temperatures and excitation temperatures generally do not show much deviation, it can be surmised that mostly thermal radiation is observed; meaning the LS-APGD behaves more like a flame source than an ICP. Based on these previously defined characteristics of the LS-APGD, flame emission spectral compilations were consulted in addition to the NIST spectral database to determine which analyte emission transitions might be expected from the LS-APGD-OES.[43, 44]

Zinc - Flame emission spectra of Zn are typically composed solely of the Zn (I) 213.9 nm emission transition.[43] While few APGD sources have been characterized by an extensive line selection study, many of these studies report quantitative characterizations of Zn at the 213.9 nm line.[33, 45] The only emission transition observed in this work was the Zn (I) line at 213.9 nm, mirroring flame emission spectra and other APGD-OES reports. The fact that no other emission transitions are observed was

expected, since the transition probability (A_{ki}) of the Zn (I) line at 213.9 nm is 7.14 10^8 s^{-1}.[44] This is nearly 2x higher than all persistent Zn (II) emission transitions. Additionally, the ionization potential of Zn is approximately 9.4 eV, meaning it is possible the plasma is not capable of ionizing Zn in large enough excited state populations for Zn (II) transitions to be observed.

In a previous LS-APGD-OES study, the Zn (II) transitions at 202.5 and 206.2 nm and Zn (I) transitions at 472.2 and 481.1 nm were reported in addition to the 213.9 nm emission line observed here.[17] That work has some key differences from this study including operating the LS-APGD in a different powering mode, using different operating conditions, and a different detector. Each of these differences would have an impact on the observed Zn emission transitions. The spectral region where Zn (II) emission transitions occur is densely populated with NO molecular bands so it is possible that the Zn (II) emission cannot overcome the high background when operated with the conditions used in this work. As for the Zn (I) emission transitions at 472.2 and 481.1 nm, no A_{ki} values are reported so it is difficult to determine if transition probabilities play a role here. Additionally, the previous work that shows detectable emission from these transitions employed a five-channel CCD detector while a monochromator/PMT setup was employed here. It is likely that the detector in the previous work had greater sensitivity for the spectral region between 470 and 485 nm than the monochromator employed in this study.

Magnesium - Typically, the Mg (I) emission transition at 285.2 nm is used for flame and APGD-OES analyses.[41, 43] However, three spectroscopic lines were observed in the spectra from this work: two Mg (II) transitions at 279.6 and 280.3 nm and the Mg

(I) transition at 285.2 nm. Interestingly, the ionic emission transitions for the Mg (II) transitions detected have lower A_{ki} (2.6 10^8 s^{-1} for both)[44] than those for the Zn (II) transitions that were not observed in this work. However, the ionization potential of Mg is lower (7.6 eV) than that of Zn (9.4 eV), and so it is reasonable to conclude that Mg is ionized in a much higher proportion than Zn.

Previous LS-APGD-OES studies report either the Mg (II) line at 280.3 nm[41] or the Mg (I) line at 285.2 nm,[46] with neither work reporting the presence of both emission transitions. Since no spectra are reported in either work and these studies were monitoring the intensity of the emission transition as opposed to identifying the ideal emission transition, it is difficult to tell if differing plasma conditions or operating modes affected the species of Mg observed.

Copper - Cu emission spectra are typically characterized by the resonant Cu (I) emission transitions at 324.7 and 327.4 nm.[43] Experiments with flame sources and other APGD sources typically utilize the 324.7 nm Cu (I) transition, likely because it is clear from atmospheric background features relative to the 327.4 nm Cu (I) transition.[33, 47] These two Cu (I) emission transitions were the only lines observed in the spectra obtained for this work. No Cu (II) emission lines were detected in this work. This closely aligns with previously reported LS-APGD-OES literature which reports only detecting the 324.7 and 327.4 nm Cu (I) emission lines.[17]

Silver - Ag emission spectra are similar to that of Cu in the fact that two prominent atomic lines are typically observed, at 328.1 and 338.3 nm.[43] This is true for both flame sources and other APGD sources.[45, 47] The emission spectra obtained for this work are no different, with only the two Ag (I) transitions at 328.1 and 338.3 nm

being detected. Similar to Cu and Zn, no Ag (II) emission transitions were detected. This data is consistent with the most recently published LS-APGD-OES works that analyzed Ag.[34, 35] Each of these studies reported only the Ag (I) emission transitions discussed here, but it should be noted that neither of these works attempted to isolate other Ag (I) or Ag (II) transitions.

Chromium - Typically, in flame sources, the Cr (I) lines at 357.9 and 425.4 nm are most often employed.[43] Similarly, work performed with the solution cathode glow discharge (SCGD) source utilized the 357.9 nm Cr (I) emission transition for quantitative determination.[48] Other APGD sources have reported the detection of six Cr (I) emission lines at 357.9, 359.3, 360.4, 425.4, 427.4, and 428.9 nm,[49] appearing as two groups in ~ 3 nm windows. It is typical for Cr (I) emission in these regions to present groups of three transitions spanning approximately 3 nm.[49] The highest energy emission transition in each region (357.9 and 425.4 nm) is typically used analytically due to the high emission intensity. In the spectra obtained for this work, this is not the case. For the first grouping of Cr (I) transitions, all three were detected. However, the Cr (I) transition at 357.9 nm was heavily interfered with by a N_2 molecular emission band. In the case of the second grouping of Cr (I) emission transitions, the expected line at 425.5 nm was also subjected to interference by N_2 emission, while the other two emission transitions in the grouping were intense and unobstructed. No previous LS-APGD studies have been performed with Cr, so no comparisons can be made.

Calcium - When analyzed by flame atomic emission spectroscopy, Ca emission spectra typically display Ca (II) emission at 393.4 and 396.9 nm and Ca (I) at 422.7 nm.[43] Previous work with other APGD sources has typically used the Ca (I) transition,

though none have reported a detailed Ca line selection.[13, 50] For this work, the spectra obtained were closer to flame emission spectra, with both of the Ca (II) emission transitions and the Ca (I) transition being observed. It is worth noting that previous APGD works did not report every detected emission line. Therefore, potential differences in the spectra obtained in this work and those cannot be assessed. By the same token, no previous LS-APGD-OES works have studied Ca emission.

Sodium - Several Na emission transitions have been observed in flame sources, including the Na (I) emission lines at 330.2, the classic 589.0/589.6 doublet, and 819.5 nm.[43] The doublet lines have been most frequently used with other APGD sources (including the LS-APGD[35]), where they typically compare their performance to ICP-OES.[51-53] Upon initial introduction of the 500 μg mL^{-1} Na solution to the LS-APGD, the intensity of the emission at 589.0 and 589.6 nm saturated the detector. Given the spectral complexity in the region, the 330.2 nm transition could not be discerned. The Na (I) 819.5 nm emission was not detected with the LS-APGD, as the throughput of this monochromator is 200 – 800 nm. Observation of the Na (II) transition has not been noted with other APGD sources.

Potassium - The final analyte determined in this study was K. When analyzed with flame sources, the resulting K spectra typically contain K (I) transitions at 404.4, 766.5, and 769.9 nm.[43] Other APGD sources have reported exclusively detecting the two transitions at 766.5 and 769.9 nm.[33, 54] No emission was observed at the 404.4 nm transition for this LS-APGD-OES. This is likely due to the low probability (0.01 10^8 s^{-1}) of the transition.[44] However, the responses of the K (I) emission at 766.5 and 769.9 nm saturated the detector. No K (II) transitions were observed in these experiments, as

would be anticipated. Previous LS-APGD literature has not reported K emission, so no parallels can be drawn.

Repeatability of Identified Analyte Lines

The analytical precision of the identified analyte lines was analyzed by performing triplicate 20 μL injections of each analyte when the plasma was sustained with a 5% HNO_3 electrolyte flow. The peak area, peak height, S/B, and S/N were calculated for each injection and the average, standard deviation, and %RSD for the set of injections determined. Good stability was defined as a precision of <10 %RSD across the triplicates.

Table 2 presents the average peak area, average peak height, average S/B and average S/N, as well as the respective %RSDs for each of the analytes. Mg is discussed here as a general example due to multiplicity of transitions monitored and the interesting trade-offs between emission intensity and %RSD. However, the same sorts of evaluation were performed for each identified emission line. The ionic emission transition at 279.6 nm has a higher average area, average peak height, and average S/N than the ionic transition at 280.3 nm, as shown in Table 2. However, the %RSDs associated with each of the metrics are higher for the 279.6 nm line than for the 280.3 nm line, save for average peak height. Therefore, the Mg (II) transition at 280.3 nm was chosen because of the higher associated precision even though the absolute values of some of the metrics were lower for the 279.6 nm line.

The analytical lines chosen for the remainder of this work, as well as the associated response statistics for each line, are presented in bold text within Table 2 for each element. The average peak area is reproducible to better than 10 %RSD in all

cases except for Zn. The Zn transition is the least stable line monitored, with high deviation in peak area, peak height, and S/N. These high deviations are likely caused by the relatively low emission intensity of the Zn (I) and the high variability of the background signal in that region. The analytical performance of Zn will not be pursued further in this work since the emission is unstable. In the future, a plasma parameterization specifically for Zn emission should be conducted to understand how to best detect emission of that species. The remainder of the analytes are very precise in terms of the statistics monitored. Interestingly, the average peak height is more reproducible than the average peak area for all analytes except for Zn. As such, average peak height was used to evaluate the analytical performance of the monitored analytes.

Analytical Performance of Monitored Elements/Transitions

After the selection of the most optimal line for each analyte, response curves were generated for the transitions highlighted in Table 2. These curves were acquired using the single-element solutions of each analyte, with each point representing the average of triplicate injections (20 μL) at that concentration. The line of best fit, R^2 values, and calculated LOD (LOD = $3\sigma_b/m$) for all calibration curves are shown in Table 3. Previously published LODs for some of the analytes monitored in this study *via* LS-APGD-OES were as follows: Cu (not determined), Ag (3.9 μg mL^{-1}), Mg (10.6 μg mL^{-1}), and Zn (4.9 μg mL^{-1}).[41] A more recent study detailing the benefits of sheathing the LS-APGD microplasma from ambient air also reported detection limits of 4.0 μg mL^{-1} for Ag and 0.08 μg mL^{-1} for Na.[35] As shown in Table 3, the LODs are improved from the previous studies in all cases except for Na. The change in analytical performance for

the improved analytes may be attributed to operational differences between the previous works and that employed here. For example, the work by Quarles Jr. *et al.* involved an operating condition parameterization regarding only the discharge current and solution flow rate, using an OVAT method.[41] More so, the detector used in that work was a polychromator equipped with a 2400 grooves mm^{-1} grating and 26 PMTs for simultaneous analysis of multiple species. As such, the previous work used a multi-element solution comprised of all analytes of interest rather than evaluating performance with a single element first; as in the case here.

The same solutions were used to generate calibration curves using a ThermoFisher Scientific (Waltham, MA) iCAP 7200 ICP-OES system within the Department of Chemistry at Clemson University. These calibration curves were acquired at the same emission lines used for the LS-APGD calibration curves, as these were in fact listed as the ideal emission lines in the ICP-OES software. The data for the ICP-OES calibration curves is also shown in Table 3. A LOD is not shown for Ca with the ICP-OES due to the large amount of carryover that was observed between acquisitions, even at low concentrations. After a 15-minute flush of 10% HNO_3, the persistent Ca emission signal was no longer detectable. However, additional attempts to generate Ca calibration curves resulted in the same carryover, resulting in the absence of ICP metrics in the table. It is immediately clear that the LODs acquired with the LS-APGD are approximately 3-4 orders of magnitude higher than those obtained with the ICP. To be fair, these differences cannot be attributed entirely to the sources themselves, as the quality of the respective spectrometers is very different. The ICP spectrometer clearly provides higher resolution, throughput, and sensitivity. Ideally, the

microplasma could be coupled to that spectrometer, but this is not possible in terms of circumventing that instrument's interlock system. However, it is important to note that each point on the calibration curves acquired *via* analysis with the LS-APGD required less than 0.1 mL of solution, whereas each point on the ICP-OES calibration curves required approximately 5 mL of solution.

In order to better compare the LODs of the two systems with respect to the intended field of use of the microplasma, calculations were performed relative to the absolute mass instead of concentration. Calculating absolute mass for the LS-APGD is simple since a syringe pump is used to control the flow rate at which solution is introduced to the plasma, and discrete injections are performed with the use of a sample loop of a known (20 μL) volume. For the ICP-OES system however, this calculation is more difficult since the sample uptake rate and volume of solution entering the plasma are not known. As such, the absolute mass was estimated using the following procedure: the sample uptake rate was estimated by monitoring how much solution was taken up by the plasma during a period of one minute. This experiment was performed ten times and the average volume used to calculate the sample uptake rate. Using this calculated sample uptake rate and the known software-specified integration time for each measurement, the absolute mass of solution used during each acquisition was calculated.

The results of the absolute mass-based calculations for the LS-APGD and ICP-OES are also shown in Table 3, with values that are now more comparable. While the LODs for the LS-APGD are still higher than ICP LODs, they are only higher by 1-2 orders of magnitude in comparison to 3-4 orders of magnitude for concentration-based

LODs. Even so, the LS-APGD could be a reasonable choice over ICP-OES for those cases where samples cannot be transported back to a laboratory (i.e., field deployment desired) or if the cost of purchasing and maintaining an ICP-OES instrument was prohibitive.

To determine how well the LS-APGD might handle various levels of dissolved solids (solute loading), calibration curves were also obtained using a multi-element solution comprised of the aforementioned analytes. Calibration curves were obtained using both the LS-APGD and the ICP-OES in the methods described above. The solutions were composed as equal concentrations of Ag, Ca, Cu, and Mg (500 μg mL^{-1}), and then of K and Na (100 μg mL^{-1}) at the six values listed for each in the caption of Table 3. Again, a calibration curve could not be acquired for Ca using the ICP-OES due to the high levels of carryover described previously. Additionally, no data is reported for Cr for either method as it tended to precipitate out of the acidic multi-element solutions.

Looking at the data in Table 4, the LODs for the analytes change when introduced as a multi-element solution. When examining the line of best fit for each analyte, the sensitivity for Ag, Mg, and Cu decreased (decreasing slope) while the spectral background levels for Ag and Mg greatly increased (increasing intercept). As expected, these data resulted in increased LODs for Ag, Mg, and Cu from the values for single-element solutions. For all other monitored analytes, the opposite was true with increased sensitivity and a decreased spectral background being observed. In the case of Ca and Na, these data resulted in a decreased LOD, as would be expected. The LODs of K remained unchanged from the single-element solution value.

The cause of the changes in LODs when introducing analyte through a multi-element solution as opposed to single-element could be due to a variety of sources; an overloading of solute into the plasma, easily ionized element (EIE) effects, or added spectral complexity. While acquiring the data at the highest concentrations, salt deposition on the counter electrode was observed, which might suggest a solute overloading effect. To this end, the added solute may result in lower overall atomization/excitation efficiency. Increasing concentrations of EIEs including the alkali/alkaline earth elements (Na, K, Ca, etc.) have been previously reported to suppress signal intensity and affect changes in the LODs across the breadth of spectrochemical devices.[2] However, prior studies with the LS-APGD showed that the source was immune to the effects of EIE from 0 – 0.1% w/v of total EIE, as the ratio of ionized to atomic emission remained unchanged with increasing EIE concentration.[55] Since the w/v% of EIE in the multi-element solution used in this work is 0.12%, it is not expected that the EIE content is affecting LS-APGD operation. However, further spectroscopic experiments specifically monitoring this effect would be required to make a more definitive statement. Finally, based on the increased y-intercepts of some analytes, it can be inferred that a higher continuous background is observed upon introduction of the multi-element solution, resulting in increased spectral complexity compared to the single-element solutions. This combined with the resolution of the monochromator employed (0.2 nm) could affect the calculated LODs for elements whose emission transitions are in cluttered regions of the spectrum. This would explain why the LOD for K was unaffected, as the emission transition is more isolated than for the other analytes studied in this work. Since ICP-OES is typically more immune to

effects from EIEs, it was expected that the LODs acquired with the ICP-OES system would remain unchanged in the transition between single- and multi-element solutions. Overall, this was true, with only the LODs of K, Mg, and Na increasing significantly. This could be due to increased ionization of these low ionization potential elements, and not necessarily an atomic emission suppression. This has been previously reported and can be attributed to the fact that EIEs affect each analyte differently.[2]

Conclusions

The DOE parameterization of the LS-APGD provided the best powering mode and the optimal conditions under which to run the LS-APGD in that powering mode. As a result of the parameterization study, the sensitivity of the LS-APGD drastically improved for the Ag test element and surpassed the performance of all previous iterations of this microplasma source. An improvement of ~30x was achieved in LOD for Ag. Additionally, performing the parameterization using the DOE method and all operating parameters allowed for the consideration of inter-parametric effects that had previously been acknowledged but not studied completely. The operating conditions extracted from the DOE showed improvements in sensitivity over previous works.

The line selection study successfully identified the viable analytical lines for eight commonly analyzed species. The best line for analytical performance determination was established by probing each potential line for each test analyte. Once the analytical line was chosen, the analytical performance for each analyte was investigated and analytical response curves were generated. Overall, when single-element solutions are used, the analytical performance of the LS-APGD is slightly inferior to an ICP-OES. It was also established that the LS-APGD LODs are affected by high dissolved solid

content, as shown in changes of various LODs upon analysis of a multi-element solution. While the mechanism of this change has not been fully elucidated, it is likely due to the plasma being overloaded with dissolved solids. The parameterization and line selection studies conducted in this work helped push the analytical performance of the LS-APGD further than other studies, as evidenced by the lower LODs to previous LS-APGD-OES publications.

In those circumstances where moderate LODs are acceptable and portability is desirable, the LS-APGD can certainly be used in place of an ICP-OES based on evidence provided here for trace metals analysis. Further improvements are necessary for the employment of the LS-APGD as an ultra-trace metal detection method, however. For example, a strong cation exchange column as a preconcentrator could be applied to affect improved LS-APGD-OES LODs for the analytes measured here.[31] Recent results have also showed that purging ambient atmosphere from the plasma can provide improved sensitivity towards many analytes,[35] and future studies could incorporate this technique as well. For those situations, the LS-APGD is a viable instrument since it shows potential for field deployment. It could also reasonably be used for at-line batch analysis due to its small size and minimal operating requirements.

Conflicts of Interest

There are no conflicts to declare.

Acknowledgements

The authors gratefully acknowledge support provided by the Defense Threat Reduction Agency, Basic Research Award #HDTRA1-14-1-0010.

References

1. G. L. Donati, R. S. Amais and C. B. Williams, *J Anal Atom Spectrom*, 2017, **32**, 1283-1296.
2. X. H and B. T. Jones, in *Encylopedia of Analytical Chemistry*, ed. R. A. Meyers, John Wiley & Sons Ltd, Chichester. 2000, pp. 9468-9485.
3. R. F. Browner and A. W. Boorn, *Anal. Chem.*, 1984, **56**, A786-&.
4. J. Franzke, K. Kunze, M. Miclea and K. Niemax, *J Anal Atom Spectrom*, 2003, **18**, 802-807.
5. T. Cserfalvi, P. Mezei and P. Apai, *J Phys D Appl Phys*, 1993, **26**, 2184-2188.
6. P. Jamroz, K. Greda and P. Pohl, *Trac-Trends Anal. Chem.*, 2012, **41**, 105-121.
7. P. Pohl, P. Jamroz, K. Swiderski, A. Dzimitrowicz and A. Lesniewicz, *Trac-Trends Anal. Chem.*, 2017, **88**, 119-133.
8. Q. Li, Z. Zhang and Z. Wang, *Anal Chim Acta*, 2014, **845**, 7-14.
9. Z. Zhang, Z. Wang, Q. Li, H. J. Zou and Y. Shi, *Talanta*, 2014, **119**, 613-619.
10. R. Manjusha, M. A. Reddy, R. Shekhar and S. Jaikumar, *J Anal Atom Spectrom*, 2013, **28**, 1932-1939.
11. P. Mezei and T. Cserfalvi, *Appl. Spectrosc. Rev.*, 2007, **42**, 573-604.
12. M. R. Webb and G. M. Hieftje, *Anal Chem*, 2009, **81**, 862-867.
13. M. R. Webb, F. J. Andrade, G. Gamez, R. McCrindle and G. M. Hieftje, *J Anal Atom Spectrom*, 2005, **20**, 1218-1225.
14. M. R. Webb, F. J. Andrade and G. M. Hieftje, *Anal Chem*, 2007, **79**, 7807-7812.
15. R. K. Marcus and W. C. Davis, *Anal Chem*, 2001, **73**, 2903-2910.
16. R. K. Marcus, B. T. Manard and C. D. Quarles, *J Anal Atom Spectrom*, 2017, **32**, 704-716.
17. S. Konegger-Kappel, B. T. Manard, L. X. Zhang, T. Konegger and R. K. Marcus, *J Anal Atom Spectrom*, 2015, **30**, 285-295.
18. B. T. Manard, J. J. Gonzalez, A. Sarkar, M. R. Dong, J. Chirinos, X. L. Mao, R. E. Russo and R. K. Marcus, *Spectrochim. Acta Part B-At. Spectrosc.*, 2014, **94-95**, 39-47.
19. R. K. Marcus, C. D. Quarles, C. J. Barinaga, A. J. Carado and D. W. Koppenaal, *Analy. Chem.*, 2011, **83**, 2425-2429.

20. E. D. Hoegg, C. J. Barinaga, G. J. Hager, G. L. Hart, D. W. Koppenaal and R. K. Marcus, *J. Anal. Atom. Spectrom.*, 2016, **31**, 2355-2362.
21. H. W. Paing and R. K. Marcus, *J Anal Atom Spectrom*, 2017, **32**, 931-941.
22. R. K. Marcus, C. Q. Burdette, B. T. Manard and L. X. Zhang, *Anal Bioanal Chem*, 2013, **405**, 8171-8184.
23. L. X. Zhang and R. K. Marcus, *J Anal Atom Spectrom*, 2016, **31**, 145-151.
24. A. J. Carado, C. D. Quarles, Jr., A. M. Duffin, C. J. Barinaga, R. E. Russo, R. K. Marcus and D. W. Koppenaal, *J. Anal. At. Spectrom.*, 2012, **27**, 385-389.
25. C. D. Quarles, J. Gonzalez, I. Choi, J. Ruiz, X. Mao, R. K. Marcus and R. E. Russo, *Spectrochim. Acta B*, 2012, **76**, 190-196.
26. K. Greda, K. Swiderski, P. Jamroz and P. Pohl, *Microchem. J.*, 2017, **130**, 7-13.
27. K. Greda, P. Jamroz and P. Pohl, *Talanta*, 2013, **108**, 74-82.
28. Q. He, Z. L. Zhu, S. H. Hu, H. T. Zheng and L. L. Jin, *Anal Chem*, 2012, **84**, 4179-4184.
29. Y. L. Yu, Z. Du, M. L. Chen and J. H. Wang, *Angew Chem Int Edit*, 2008, **47**, 7909-7912.
30. A. J. Schwartz, K. L. Williams, G. M. Hieftje and J. T. Shelley, *Anal Chim Acta*, 2017, **950**, 119-128.
31. K. A. Hall, L. W. Jiang and R. K. Marcus, *J Anal Atom Spectrom*, 2017, **32**, 2463-2468.
32. R. J. C. Brown and M. J. T. Milton, *Trac-Trend Anal Chem*, 2005, **24**, 266-274.
33. P. Jamroz, P. Pohl and W. Zyrnicki, *J Anal Atom Spectrom*, 2012, **27**, 1032-1037.
34. K. A. Hall, H. W. Paing, M. R. Webb and R. K. Marcus, *Spectrochim. Acta Part B-At. Spectrosc.*, 2019, **154**, 33-42.
35. H. W. Paing, K. A. Hall and R. K. Marcus, *Spectrochim. Acta Part B-At. Spectrosc.*, 2019, **155**, 99-106.
36. W. C. Davis and R. K. Marcus, *Spectrochim Acta B*, 2002, **57**, 1473-1486.
37. K. Park and J. H. Ahn, *J Mater Process Tech*, 2004, **146**, 221-227.
38. B. K. Rout and R. K. Mittal, *Robot Cim-Int Manuf*, 2008, **24**, 239-248.

39. M. L. Weese, P. J. Ramsey and D. C. Montgomery, *Appl Stoch Model Bus*, 2018, **34**, 244-255.
40. B. Jones and C. J. Nachtsheim, *J Qual Technol*, 2011, **43**, 1-15.
41. C. D. Quarles, B. T. Manard, C. Q. Burdette and R. K. Marcus, *Microchem. J.*, 2012, **105**, 48-55.
42. T. Belmonte, C. Noel, T. Gries, J. Martin and G. Henrion, *Plasma Sources Sci T*, 2015, **24**.
43. C. T. J. Alkemade, T. Hollander, W. Snelleman and P. J. T. Zeegers, *Metal Vapours in Flames*, Pergamon Press Ltd., Oxford, England. 1982.
44. NIST, ed. NIST, NIST, Web. 2018, vol. 2019, ch. 1979.
45. J. M. Wang, P. F. Tang, P. C. Zheng and X. Zhai, *J Anal Atom Spectrom*, 2017, **32**, 1925-1931.
46. W. C. Davis and R. K. Marcus, *J Anal Atom Spectrom*, 2001, **16**, 931-937.
47. T. A. Doroski, A. M. King, M. P. Fritz and M. R. Webb, *J Anal Atom Spectrom*, 2013, **28**, 1090-1095.
48. J. X. Ma, Z. Wang, Q. Li, R. Y. Gai and X. H. Li, *J. Analy. At. Spectrom.*, 2014, **29**, 2315-2322.
49. P. Jamroz, K. Greda, P. Pohl and W. Zyrnicki, *Plasma Chem Plasma P*, 2014, **34**, 25-37.
50. M. R. Webb, F. J. Andrade and G. M. Hieftje, *J Anal Atom Spectrom*, 2007, **22**, 766-774.
51. M. R. Webb, F. J. Andrade and G. M. Hieftje, *Anal Chem*, 2007, **79**, 7899-7905.
52. J. L. Venzie and R. K. Marcus, *Anal. Bioanal. Chem.*, 2005, **381**, 96-98.
53. Q. He, Z. L. Zhu and S. H. Hu, *Appl Spectrosc Rev*, 2014, **49**, 249-269.
54. S. Liu, Y. Cai, Y. L. Yu and J. H. Wang, *J Anal Atom Spectrom*, 2017, **32**, 1739-1745.
55. J. L. Venzie and R. K. Marcus, *Spectrochim. Acta Part B-At. Spectrosc.*, 2006, **61**, 715-721.

Figure Captions

Fig. 1. Diagram of the LS-APGD-OES apparatus used for this work. Specific components described in text. The focal length of f_1 was 150 mm while the focal length of f_2 was 40 mm.

Fig. 2. Diagrammatic representations of the four possible LS-APGD powering modes. Solution grounded cathode (SGC) and solution powered anode (SPA) are created when the power supply is operated in the positive output mode while solution grounded anode (SGA) and solution powered cathode (SPC) are acquired when the power supply is operated in the negative output mode.

Fig. 3. a) The average signal intensity of Ag (I) 328.1 nm, b) S/B, and c) S/N of triplicate 50 μL injections of 500 μg mL^{-1} Ag, acquired at the optimized conditions for each powering mode. The error bars represent standard deviation across the three injections.

Fig. 4. Calibration curves obtained at the operating conditions found to be optimal in this work (purple), the work of Hall *et al.*[31] (orange), and the work of Marcus *et al.*[15] (grey). For this work, the points on the calibration curve are the average of three 20 μL injections and the error bars represent the standard deviation of those intensities. The previous works extend the concentration range to 500 μg mL^{-1} but this work cuts off at 250 μL mL^{-1} due to saturation of the detector at 500 μg mL^{-1}.

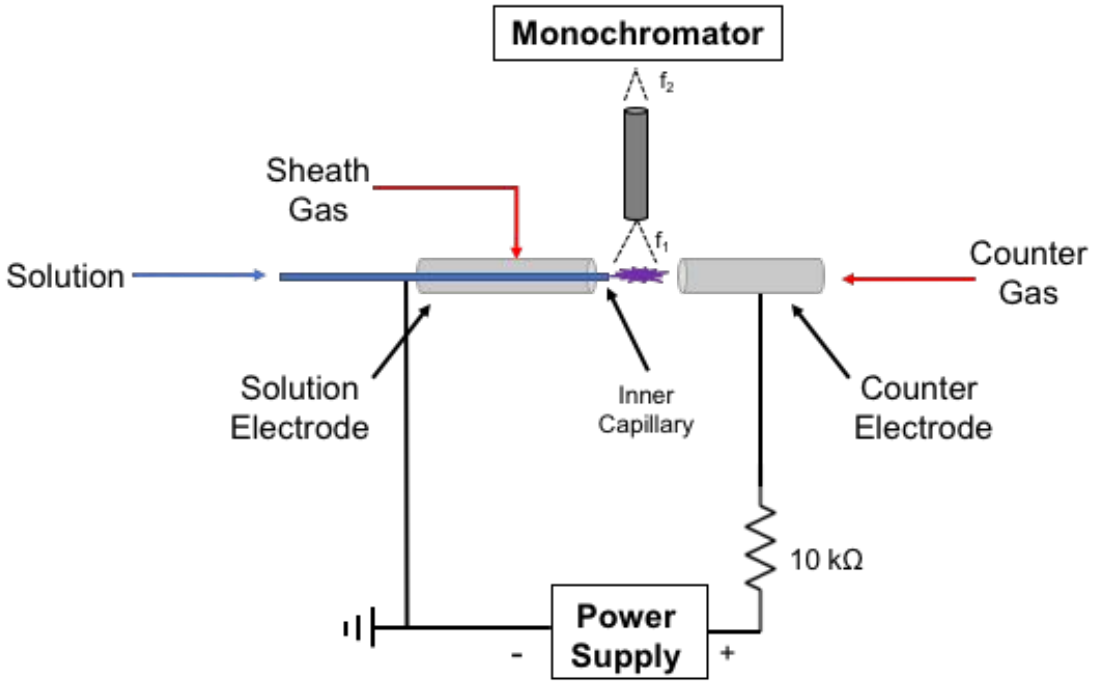
Monochromator
f2
Sheath
Gas
f1
Solution
Counter
Gas
Solution
Electrode
Inner
Capillary
Counter
Electrode
10 kΩ
Power
Supply
-
+

Fig. 1

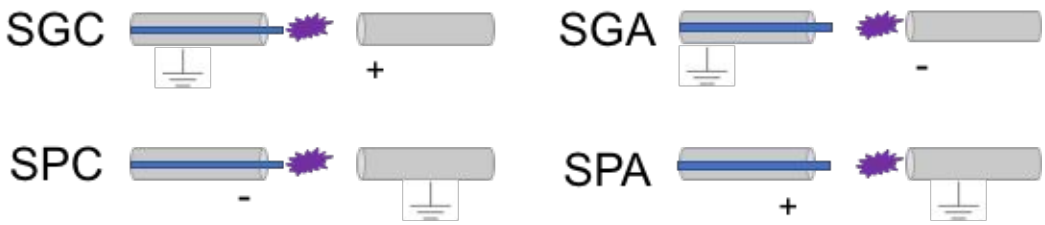
SGC
+
SGA
-
SPC
-
SPA
+

Fig. 2

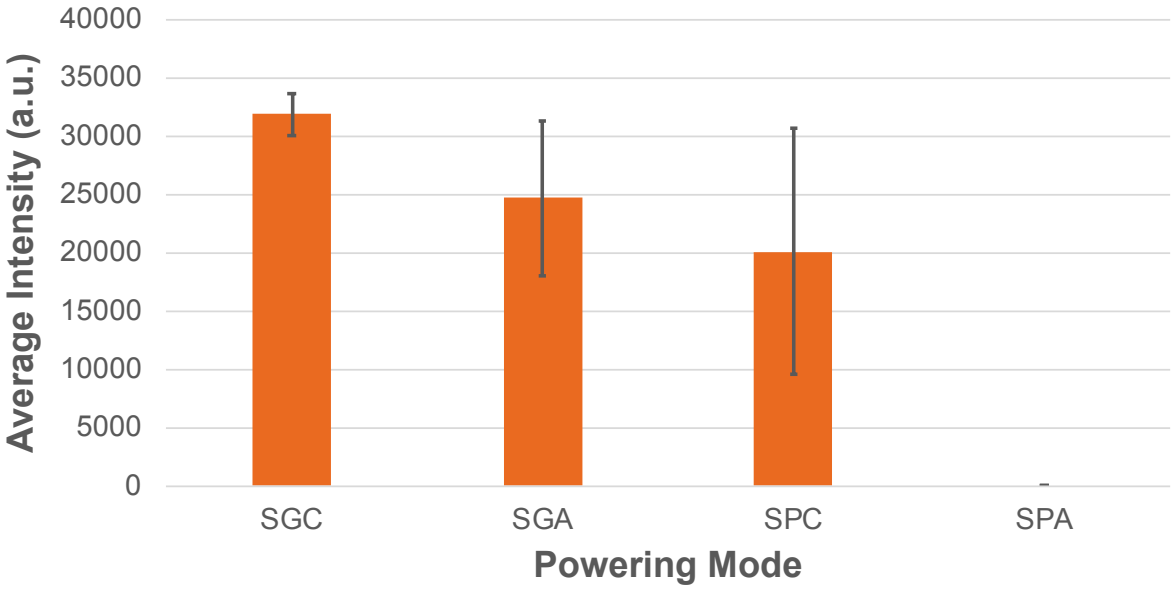
Average Intensity (a.u.)
40000
35000
30000
25000
20000
15000
10000
5000
0
SGC
SGA
SPC
SPA
Powering Mode

Fig. 3a

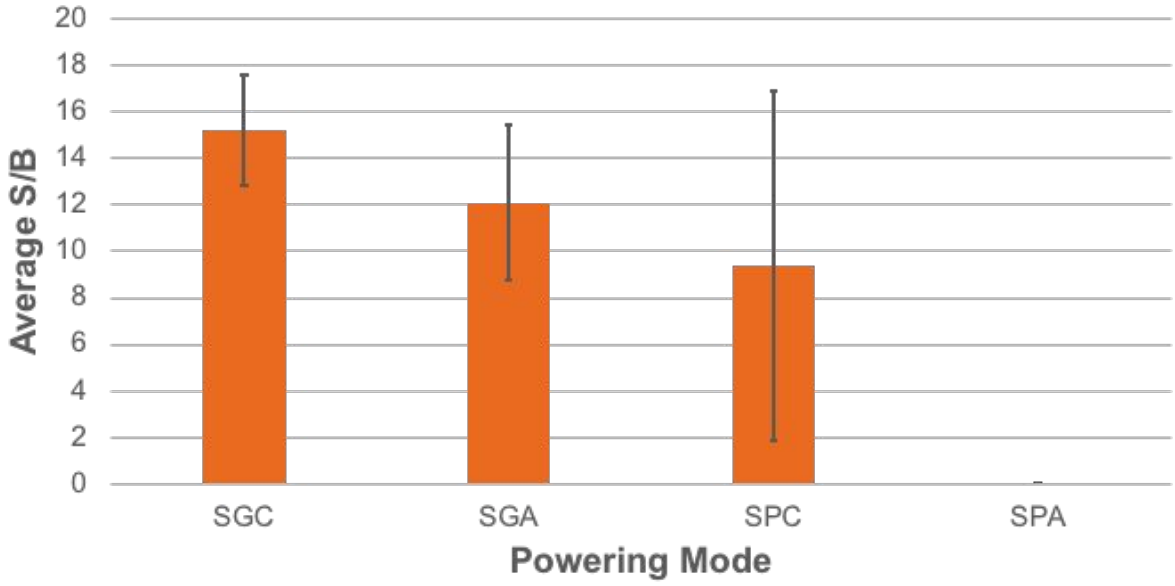
Average S/B
20
18
16
14
12
10
8
6
4
2
0
SGC
SGA
SPC
SPA
Powering Mode

Fig. 3b

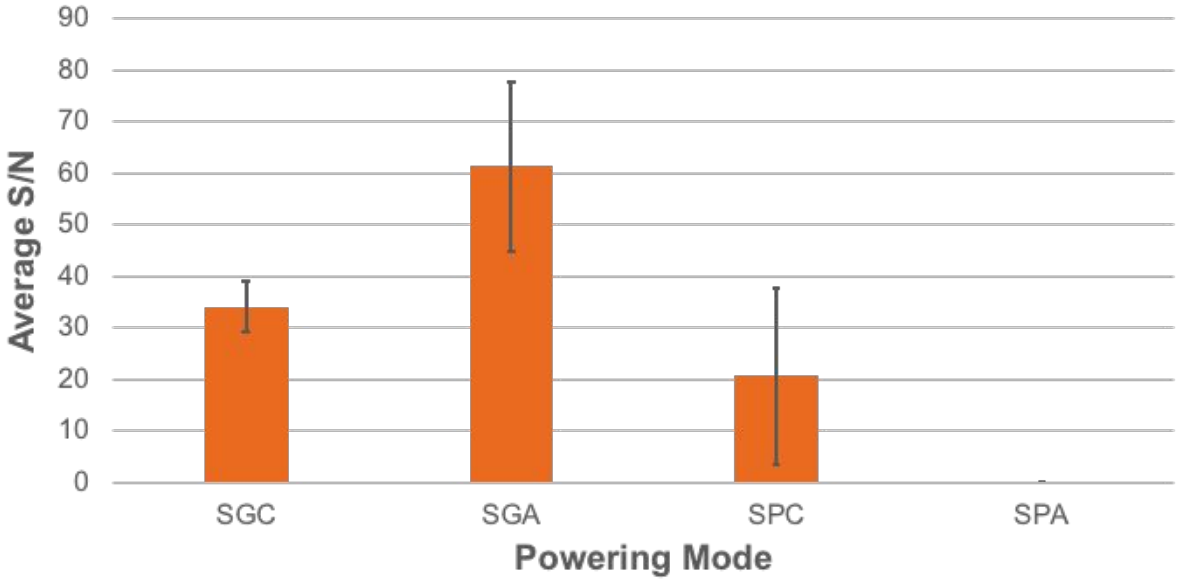
90
80
70
60
50
40
30
20
10
0
Average S/N
SGC
SGA
SPC
SPA
Powering Mode

Fig. 3c

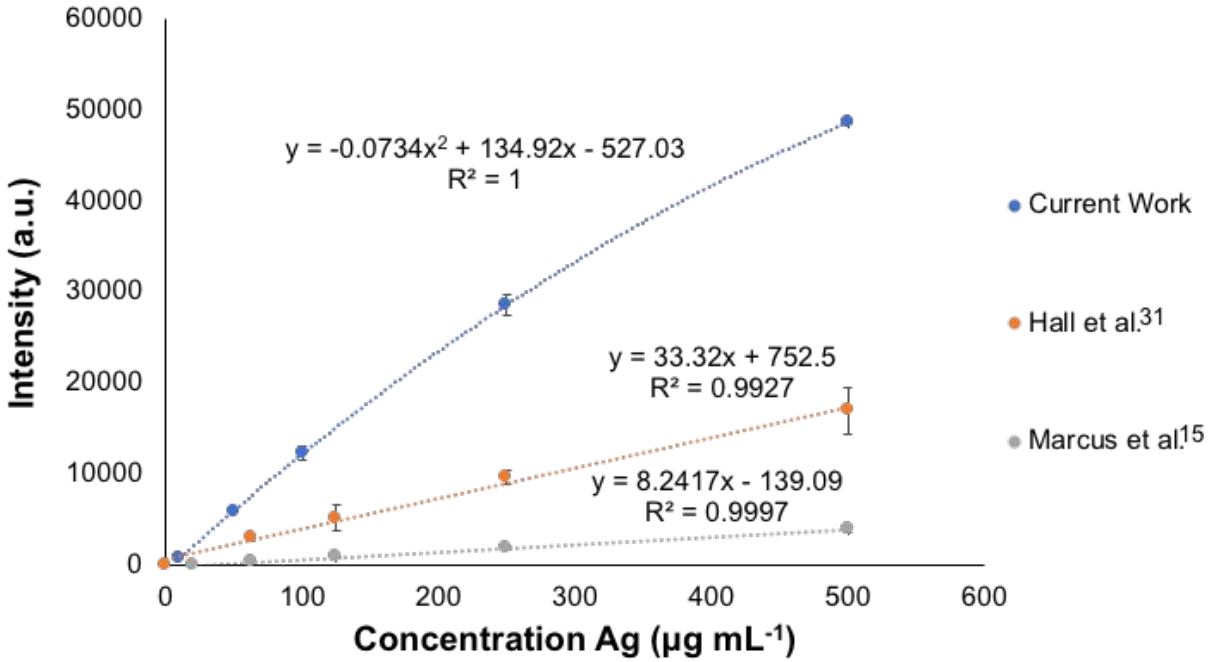
60000
50000
40000
30000
20000
10000
0
Intensity (a.u.)
y = -0.0734x² + 134.92x - 527.03
R² = 1
y = 33.32x + 752.5
R² = 0.9927
y = 8.2417x - 139.09
R² = 0.9997
0
100
200
300
400
500
600
Concentration Ag (µg mL-1)
Current Work
Hall et al.31
Marcus et al.15

Fig. 4

Table 1. JMP Pro DOE Experimental Plan. The plasma was operated at the conditions specified for each run and triplicate injections of Ag test solution were performed. The average intensity, S/B, and S/N were calculated for the injections performed at each run and input into the JMP Pro software for statistical analysis. This experimental plan was used for each powering mode.

Run	Electrode Gap (mm)	Discharge Current (mA)	Solution Flow Rate (μL min^{-1})	Sheath Gas Flow Rate (L min^{-1})	Counter Gas Flow Rate (L min^{-1})
1	3	60	100	0.8	0.2
2	0.5	30	125	0.9	0.1
3	4	30	125	0.5	0.1
4	4	30	50	0.5	0.3
5	0.5	70	25	0.9	0.1
6	4	70	125	0.5	0.4
7	0.5	30	25	0.5	0.5
8	4	70	25	0.9	0.5
9	1	40	50	0.6	0.1
10	4	30	50	0.5	0.3
11	0.5	30	125	0.5	0.3
12	0.5	70	75	0.5	0.5
13	3	40	100	0.6	0.5
14	1	70	125	0.9	0.5
15	1	40	50	0.8	0.4
16	4	30	125	0.9	0.4
17	2	60	25	0.6	0.3
18	4	30	25	0.9	0.1
19	3	60	100	0.8	0.2
20	0.5	70	125	0.5	0.1
21	4	70	50	0.5	0.1
22	1	40	50	0.8	0.4

Table 2. Average peak area, maximum emission intensity, S/B, S/N, and the corresponding %RSDs for these responses for all three visible Mg lines. Mg is shown here as a test case due to the concession made between high intensity with high %RSD and low intensity with a more acceptable %RSD.

Analyte	Line (nm)	Average Peak Area (counts*min)	%RSD Average Peak Area	Average Peak Height (a.u.)	%RSD Average Peak Height	Average S/B	%RSD Average S/B	Average S/N	%RSD Average S/N
Ag	**328.1**	**77774.5**	**10.9**	**53672.7**	**<1**	**1.1**	**1.1**	**62.5**	**3.1**
Ag	338.3	65687.5	9.5	53199.0	<1	1.0	<1	62.2	4.2
Ca	393.4	280427.0	11.2	24413.9	6.2	2.8	6.2	196.3	6.2
Ca	**396.9**	**218670.8**	**6.7**	**34661.7**	**<1**	**1.7**	**<1**	**36.3**	**7.1**
Ca	422.7	25584.7	10.5	22642.6	4.9	2.9	4.9	284.3	4.9
Cr	357.9	57513.3	25.4	18020.2	22.8	2.4	2.8	66.6	2.9
Cr	359.3	49014.8	48.3	11836.2	33.2	1.6	3.3	43.7	2.4
Cr	**360.4**	**40475.3**	**4.6**	**34245.7**	**<1**	**1.3**	**1.1**	**30.2**	**1.4**
Cr	427.4	18321.6	47.3	8772.7	80.4	1.2	8.4	32.4	9.4
Cu	**324.7**	**24298.3**	**7.2**	**37409.3**	**1.2**	**1.5**	**14.1**	**52.2**	**8.0**
Cu	327.5	32340.1	28.2	19580.4	16.3	7.7	2.9	632.6	9.4
K	766.5	11081.2	18.4	12319.9	14.5	5.2	1.5	34.9	1.5
K	**769.9**	**19007.3**	**9.4**	**24949.5**	**4.8**	**2.0**	**1.4**	**24.7**	**2.3**
Mg	279.6	20065.2	10.5	35208.1	< 1	3.8	4.9	54.3	13.1
Mg	**280.3**	**12120.9**	**5.5**	**34381.8**	**< 1**	**3.9**	**6.3**	**30.2**	**6.6**
Mg	285.2	17751.8	28.7	35278.5	< 1	2.0	6.3	22.8	4.2
Na	**589.0**	**40040.7**	**1.5**	**33477.3**	**<1**	**1.7**	**<1**	**23.8**	**4.7**
Na	589.6	31147.4	26.6	27748.7	<1	4.7	10.1	13.0	10.6
Zn	**213.8**	**2462.9**	**13.2**	**6721.9**	**22.5**	**1.0**	**2.2**	**9.9**	**85.9**

Table 3. Line of best fit, R^2 value, and calculated LOD from each calibration curve acquired using single-element analyte solutions with the LS-APGD and ICP-OES. The LS-APGD calibration curves are representative of the average emission intensity of three 20 μL injections at each concentration while the ICP-OES calibration curves are representative of the average emission intensity of three acquisitions at each concentration. The concentrations of analyte used in all calibration curves except Na and K were 10, 50, 100, 250, 400, and 500 μg mL^{-1}. The concentrations of analyte used for Na and K were 2, 10, 20, 50, 80, and 100 μg mL^{-1}.

Analyte	LS-APGD	R^2	LOD (μg mL^{-1})	LOD (ng)	ICP – OES	R^2	LOD (μg mL^{-1})	LOD (ng)
Ag	y = 64.0x - 146.7	0.9961	0.8	16	y = 2075.1x + 9478.3	0.9989	0.004	8
Ca	y = 60.8x + 786.7	0.9872	6.1	122	--	--	--	--
Cr	y = 54.8x - 9646.5	0.9969	14.8	296	y = 2323x + 9247.8	0.9993	0.002	4
Cu	y = 41.3x + 3304.5	0.9885	2.4	48	y = 2059.1x + 5753.8	0.9996	0.005	10
K	y = 47.4x + 72.4	0.9993	2.1	42	y = 740.19x + 13.619	0.9999	0.005	10
Mg	y = 40.8x - 812.4	0.9978	2.5	50	y = 18123x + 380781	0.9869	0.002	20
Na	y = 300.7x + 5286.5	0.9722	2.0	40	y = 5946.9x + 1911.9	0.9998	0.010	2

Table 4. Line of best fit, R^2 value, and calculated LOD from each calibration curve acquired using the multi-element solution with the LS-APGD and ICP-OES. The calibration curves are representative of the average emission intensity of five 20 μL injections at each concentration. The ICP-OES calibration curves show the average intensity over three acquisitions of each solution. The concentrations of analytes in the multi-element solution are detailed in the experimental section and in the caption of Table 3.

Analyte	LS-APGD	R^2	LOD ($\mu g\ mL^{-1}$)	LOD (ng)	ICP-OES	R^2	LOD ($\mu g\ mL^{-1}$)	LOD (ng)
Ag	y = 30.4x + 2858.6	0.9961	7.2	144	y = 5932.3x + 48745.0	0.9927	0.003	6
Ca	y = 79.1x + 180.3	0.9899	3.0	60	--	--	--	--
Cu	y = 35.4x + 592.9	0.9907	9.0	180	y = 2222.2x + 15695.0	0.9983	0.003	6
K	y = 101.3x - 225.5	0.9927	1.9	38	y = 685.12x + 221.6	0.9999	0.04	80
Mg	y = 14.6x + 1889.3	0.9948	7.2	144	y = 15.476x + 574.8	0.9879	2.0	4000
Na	y = 1166.7x - 386.4	0.9955	1.1	22	y = 4720.5x + 1223.4	0.9999	0.04	80

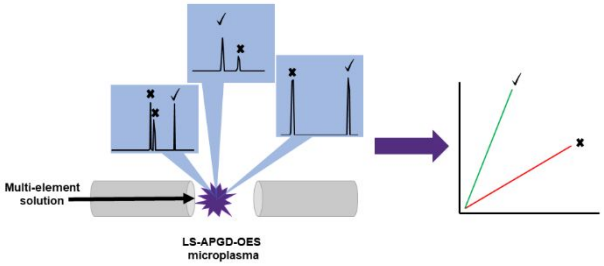

A design of experiment parameterization and line selection study was successful in improving LS-APGD-OES analytical performance.